6-20-2012

Comprehensive Solution to Scattering by Bianisotropic Objects of Arbitrary Shape

Chong Mei
Syracuse University

Moamer Hasanovic
Syracuse University

Jay K. Lee
Syracuse University, leejk@syr.edu

Ercument Arvas
Syracuse University, earvas@syr.edu

Progress In Electromagnetics Research B, Vol. 42, 335–362, 2012

COMPREHENSIVE SOLUTION TO SCATTERING BY BIANISOTROPIC OBJECTS OF ARBITRARY SHAPE

C. Mei, M. Hasanovic*, J. K. Lee, and E. Arvas

Department of Electrical Engineering and Computer Science, Syracuse University, Syracuse, NY 13244, USA

Abstract—This paper presents a method of moments (MoM) solution for the problems of electromagnetic scattering by inhomogeneous three-dimensional bianisotropic scatterers of any shape. The electromagnetic response of bianisotropy has been described by the constitutive relations of the most general form composed of four 3×3 matrices or tensors. The volume equivalence principle is used to obtain a set of mixed potential formulations for a proper description of the original scattering problem. Here, the total fields are separated into the incident fields and the scattered fields. The scattered fields are related to the electric and magnetic potentials which are excited by electric and magnetic bound charges and polarization currents. The body of the scatterer is meshed through the use of tetrahedral cells with face-based functions used to expand unknown quantities. At last, the Galerkin test method is applied to create a method of moments (MoM) matrix from which the numerical solution is obtained. Implemented in a MATLAB program, the numerical formulation is evaluated and verified for various types of scatterers. The results are compared with those of previous work, and a good agreement is observed. Finally, a scattering from a two-layered dispersive chiroferrite sphere is presented as the most general example.

1. INTRODUCTION: BIANISOTROPIC MATERIALS

Study of bianisotropic materials, their properties and interaction with electromagnetic fields is one of the main research areas that attract electromagnetic community in recent years. Rapid evolution of material technology has triggered the demand for applications of complex media and further revitalized the interest of the researchers

Received 20 June 2012, Accepted 23 July 2012, Scheduled 24 July 2012

* Corresponding author: Moamer Hasanovic (mhasanov@syr.edu).

in this particular field. Dielectric crystals and polymers are being used in many electronic and optical devices. Magnetic anisotropy has always played an important role in ferromagnetic film circuits [1]. Recent research indicates that chiral materials, as well as biisotropic materials, are being investigated for various applications such as antenna radomes [2], waveguides [3], polarization transformers [4], and microstrip circuit materials [5]. Other complex types of media, such as chiroferrites, which are combinations of chiral materials and ferrites, as well as Faraday chiral materials, are also studied [6, 7]. In general, anisotropic and bianisotropic materials are being researched as substrates for microstrip antennas, RF circuits, and MMICs [8–11], and as radar absorbers in anechoic chambers [12]. A study of electromagnetic scattering by inhomogeneous bianisotropic bodies is also important for applications such as detection of airborne particulates, medical diagnostics, power absorption in biological bodies and performance study of antennas.

The concept of bianisotropy has two origins. First, it is a generalization of the concept of anisotropy, and secondly, it is an extension of the magnetoelectric coupling property possessed by media such as isotropic chiral materials. The media that can be classified into a general category of bianisotropic media include gyrotropic media, biisotropic chiral media, Faraday chiral media, and moving media.

Macroscopic electromagnetics provides a description of a certain material medium through constitutive relations. Constitutive relations characterize the material properties that govern the interaction between electromagnetic waves and the media. Once these relations have been formulated, the solution of the electromagnetic field problem is reduced to a set of partial differential equations with certain boundary conditions.

For linear and stationary media, the constitutive relations in the most general form can be described by the following set of equations,

$$\begin{aligned} \bar{D} &= \bar{\bar{\varepsilon}} \cdot \bar{E} + \bar{\bar{\xi}} \cdot \bar{H} \\ \bar{B} &= \bar{\bar{\zeta}} \cdot \bar{E} + \bar{\bar{\mu}} \cdot \bar{H} \end{aligned} \tag{1}$$

where $\bar{\bar{\varepsilon}}$ is the permittivity tensor, $\bar{\bar{\mu}}$ is the permeability tensor, and $\bar{\bar{\xi}}$, and $\bar{\bar{\zeta}}$ are the magnetoelectric tensors. In this paper, the overbar $^{-}$ denotes a vector and the double overbar $^{=}$ denotes a tensor.

A medium is *bianisotropic* when these tensors are all assumed to be generalized 3×3 matrices or tensors. One of the fundamental properties of bianisotropic media is the cross-coupling between the electric and magnetic fields. This means that, when placed in an electric or magnetic field, a bianisotropic medium becomes both polarized and magnetized.

If the tensors are in the form of $\bar{\bar{\varepsilon}} = \varepsilon \cdot \bar{\bar{I}}$, $\bar{\bar{\mu}} = \mu \cdot \bar{\bar{I}}$, $\bar{\bar{\xi}} = \xi \cdot \bar{\bar{I}}$, and $\bar{\bar{\zeta}} = \zeta \cdot \bar{\bar{I}}$, where ε, μ, ξ, and ζ are scalars and $\bar{\bar{I}}$ is the unit tensor, the medium is *biisotropic*, and its constitutive relations can be written as

$$\begin{aligned} \bar{D} &= \varepsilon \bar{E} + \xi \bar{H} \\ \bar{B} &= \zeta \bar{E} + \mu \bar{H}. \end{aligned} \tag{2}$$

If ξ and ζ are zero, and ε and μ are non-zero scalars, the medium is simply an isotropic medium, and $\bar{E}$ is parallel to $\bar{D}$ and $\bar{H}$ is parallel to $\bar{B}$.

As shown in the definitions above, all linear and stationary media, isotropic or anisotropic, biisotropic or bianisotropic, can be treated as bianisotropic or special cases of bianisotropic media.

With the development of material techniques, there is an urgent need for a fast and accurate general-purpose electromagnetic field solver that could handle all kinds of inhomogeneity, dispersion, anisotropy, chirality, and even bianisotropy. There exist several methodologies to analyze electromagnetic field interaction with complex media. For example, analytical methods such as Mie series expansion [13] and a matrix technique [14] are successfully used to study source radiation and wave propagation problems in simple structures such as biisotropic spheres or bianisotropic multilayer transmission lines. Three dimensional (3D) full-wave numerical algorithms in the time domain such as finite-difference time-domain (FDTD) method, the method of line (MoL), and transmission line modeling method (TLM) have been extended to model electromagnetic interaction with complex materials such as chiral materials and gyrotropic materials [15–17]. More recent research efforts are related to scattering from homogeneous dispersive anisotropic and biisotropic materials. However, each of these methods has certain limitations. Analytical methods are difficult to apply to complex structures that involve 3D arbitrarily shaped geometries. When solving problems that involve dispersive materials, time domain methods rely on the Z-transform of analytical expressions that describe the dispersion properties of a material [18]. These analytical expressions are in many cases very difficult to obtain. Corresponding computer programs also need to be adapted for the different dispersion properties of the material. Current frequency domain methods such as finite-element method (FEM), FEM-boundary element method (FEM-BEM) [19–21], and method of moments (MoM) are also able to treat wave propagation and radiation problems related to chiral media or anisotropic materials. Generally, problems are solved in frequency domain, so there is no need to obtain analytic expressions of the material dispersion in advance.

In general, there has been little research work in solving problems

that involve general bianisotropic materials. The main purpose of this paper is to offer a method of moments solution to problems that involve 3D inhomogeneous bianisotropic scatterers of an arbitrary shape. The developed formulation does not put any limits on the geometrical assignment of material properties to the scatterer. It can be applied to multilayered scatterers, and scatterers with materials assigned to different regions of the scatterer in a linear, exponential or any other fashion, etc..

2. FORMULATION OF THE PROBLEM

Let us consider an inhomogeneous bianisotropic body of arbitrary three-dimensional shape characterized by the constitutive relations (1).

As shown in Figure 1, if the body is illuminated by a time-harmonic electromagnetic wave with $e^{j\omega t}$ dependence, the fields in the body are described by Maxwells equations as [22]

$$\begin{aligned} \nabla \cdot \bar{E} &= \frac{\rho_{eb}}{\varepsilon_0} \\ \nabla \cdot \bar{H} &= \frac{\rho_{mb}}{\mu_0} \\ \nabla \times \bar{E} &= -j\omega\mu_0 \bar{H} - \bar{J}_{mp} \\ \nabla \times \bar{H} &= j\omega\varepsilon_0 \bar{E} + \bar{J}_{ep} \end{aligned} \tag{3}$$

where $\bar{J}_{ep}$ and $\bar{J}_{mp}$ are the electric and magnetic polarization currents, and the ρ_{eb} and ρ_{mb} are electric bound charges and magnetic bound charges, respectively. Bound charge densities and polarization current densities are related to the electric and magnetic polarizations by

$$\begin{aligned} \rho_{eb} &= -\nabla \cdot \bar{P} \\ \rho_{mb} &= -\mu_0 \nabla \cdot \bar{M} \\ \bar{J}_{ep} &= j\omega \bar{P} \\ \bar{J}_{mp} &= j\omega\mu_0 \bar{M} \end{aligned} \tag{4}$$

where $\bar{P}$ and $\bar{M}$ represent electric polarization and magnetic polarization (magnetization) of the bianisotropic scatterer, respectively, and given by:

$$\begin{aligned} \bar{P} &= \bar{D} - \varepsilon_0 \bar{E} \\ \bar{M} &= \frac{1}{\mu_0} \bar{B} - \bar{H}. \end{aligned} \tag{5}$$

The total fields $\bar{E}$ and $\bar{H}$ can be separated into two components: the incident field component ($\bar{E}^{inc}$, $\bar{H}^{inc}$) produced by the primary

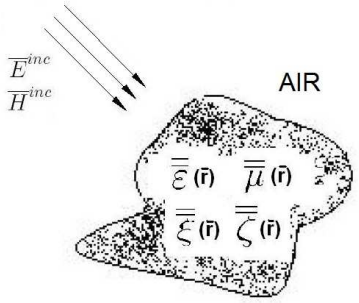

Figure 1. Inhomogeneous bianisotropic body in free space illuminated by an electromagnetic wave.

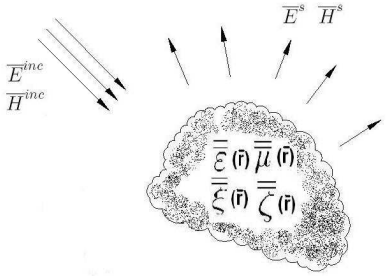

Figure 2. Incident field and scattered field.

sources and the scattered component ($\bar{E}^s$, $\bar{H}^s$) produced as a result of scattering from the bianisotropic body, as shown in Figure 2.

Hence, one can write the total fields as

$$\begin{aligned} \bar{E} &= \bar{E}^s + \bar{E}^{inc} \\ \bar{H} &= \bar{H}^s + \bar{H}^{inc} \end{aligned} \tag{6}$$

where the known incident fields $\bar{E}^{inc}$ and $\bar{H}^{inc}$ satisfy

$$\begin{aligned} \nabla \cdot \bar{E}^{inc} &= 0 \\ \nabla \cdot \bar{H}^{inc} &= 0 \\ \nabla \times \bar{E}^{inc} &= -j\omega\mu_0 \bar{H}^{inc} \\ \nabla \times \bar{H}^{inc} &= j\omega\varepsilon_0 \bar{E}^{inc} \end{aligned} \tag{7}$$

and the unknown scattered fields $\bar{E}^s$ and $\bar{H}^s$ satisfy

$$\begin{aligned} \nabla \cdot \bar{E}^s &= \frac{\rho_{eb}}{\varepsilon_0} \\ \nabla \cdot \bar{H}^s &= \frac{\rho_{mb}}{\mu_0} \\ \nabla \times \bar{E}^s &= -j\omega\mu_0 \bar{H}^s - \bar{J}_{mp} \\ \nabla \times \bar{H}^s &= j\omega\varepsilon_0 \bar{E}^s + \bar{J}_{ep}. \end{aligned} \tag{8}$$

To solve for the scattered field, one can break the scattered field into two parts, namely,

$$\begin{aligned} \bar{E}^s &= \bar{E}^s_1 + \bar{E}^s_2 \\ \bar{H}^s &= \bar{H}^s_1 + \bar{H}^s_2 \end{aligned} \tag{9}$$

where $\bar{E}_1^s$ and $\bar{H}_1^s$ are the fields generated by the electric charges and electric currents only, and $\bar{E}_2^s$ and $\bar{H}_2^s$ are the fields generated by the magnetic charges and magnetic currents only.

$\bar{E}_1^s$ and $\bar{H}_1^s$ satisfy

$$\begin{aligned} \nabla \cdot \bar{E}_1^s &= \frac{\rho_{eb}}{\varepsilon_0} \\ \nabla \cdot \bar{H}_1^s &= 0 \\ \nabla \times \bar{E}_1^s &= -j\omega\mu_0 \bar{H}_1^s \\ \nabla \times \bar{H}_1^s &= j\omega\varepsilon_0 \bar{E}_1^s + \bar{J}_{ep}. \end{aligned} \tag{10}$$

$\bar{E}_2^s$ and $\bar{H}_2^s$ satisfy

$$\begin{aligned} \nabla \cdot \bar{E}_2^s &= 0 \\ \nabla \cdot \bar{H}_2^s &= \frac{\rho_{mb}}{\mu_0} \\ \nabla \times \bar{E}_2^s &= -j\omega\mu_0 \bar{H}_2^s - \bar{J}_{mp} \\ \nabla \times \bar{H}_2^s &= j\omega\varepsilon_0 \bar{E}_2^s. \end{aligned} \tag{11}$$

The solutions of Equation (10) can be obtained by introducing the magnetic vector potential $\bar{A}$ and the electric scalar potential V, so that

$$\begin{aligned} \bar{E}_1^s &= -j\omega\bar{A} - \nabla V \\ \bar{H}_1^s &= \frac{1}{\mu_0} \nabla \times \bar{A}. \end{aligned} \tag{12}$$

Using Green's function in free space $G(\bar{r}, \bar{r}')$

$$G(\bar{r}, \bar{r}') = \frac{e^{-jk_0|\bar{r}-\bar{r}'|}}{4\pi|\bar{r}-\bar{r}'|}\ , \tag{13}$$

where k_0 is the wavenumber in free space, defined as $k_0 = \omega\sqrt{\varepsilon_0\mu_0}$, $\bar{r}$ the position vector of the field point, $\bar{r}'$ the position vector of the source point, and $\bar{A}$ and V can be expressed in terms of the polarization current and the bound charge density as

$$\bar{A} = \mu_0 \int_V \bar{J}_{ep}(\bar{r}') G(\bar{r}, \bar{r}') dv' \tag{14}$$

$$V = \frac{1}{\varepsilon_0} \int_V \rho_{eb}(\bar{r}') G(\bar{r}, \bar{r}') dv' \tag{15}$$

$\bar{A}$ and V are related by the Lorentz gauge

$$\nabla \cdot \bar{A} + j\omega\varepsilon_0\mu_0 V = 0. \tag{16}$$

Similarly, Equation (11) can be solved by introducing electric vector potential $\bar{F}$ and magnetic scalar potential U

$$\begin{aligned} \bar{H}_2^s &= -j\omega\bar{F} - \nabla U \\ \bar{E}_2^s &= -\frac{1}{\varepsilon_0}\nabla \times \bar{F}. \end{aligned} \tag{17}$$

$\bar{F}$ and U can be expressed in terms of the magnetic polarization current and the bound magnetic charge density as

$$\bar{F} = \varepsilon_0 \int_V \bar{J}_{mp}\left(\bar{r}'\right) G\left(\bar{r}, \bar{r}'\right) dv' \tag{18}$$

$$U = \frac{1}{\mu_0} \int_V \rho_{mb}\left(\bar{r}'\right) G\left(\bar{r}, \bar{r}'\right) dv'. \tag{19}$$

$\bar{F}$ and U are related by

$$\nabla \cdot \bar{F} + j\omega\varepsilon_0\mu_0 U = 0. \tag{20}$$

The total scattered fields then can be written as

$$\begin{aligned} \bar{E} &= \bar{E}^{inc} - j\omega\bar{A} - \nabla V - \frac{1}{\varepsilon_0}\nabla \times \bar{F} \\ \bar{H} &= \bar{H}^{inc} - j\omega\bar{F} - \nabla U + \frac{1}{\mu_0}\nabla \times \bar{A}. \end{aligned} \tag{21}$$

Note that when the surface charges σ_{eb} and σ_{mb} are present on the boundary, the surface integrals must also be evaluated and added to find V and U.

$$\bar{A} = \mu_0 \int_V \bar{J}_{ep}\left(\bar{r}'\right) G\left(\bar{r}, \bar{r}'\right) dv' \tag{22}$$

$$V = \frac{1}{\varepsilon_0} \int_V \rho_{eb}\left(\bar{r}'\right) G\left(\bar{r}, \bar{r}'\right) dv' + \frac{1}{\varepsilon_0} \int_S \sigma_{eb}\left(\bar{r}'\right) G\left(\bar{r}, \bar{r}'\right) ds' \tag{23}$$

$$\bar{F} = \varepsilon_0 \int_V \bar{J}_{mp}\left(\bar{r}'\right) G\left(\bar{r}, \bar{r}'\right) dv' \tag{24}$$

$$U = \frac{1}{\mu_0} \int_V \rho_{mb}\left(\bar{r}'\right) G\left(\bar{r}, \bar{r}'\right) dv' + \frac{1}{\mu_0} \int_S \sigma_{mb}\left(\bar{r}'\right) G\left(\bar{r}, \bar{r}'\right) ds'. \tag{25}$$

Following the flow chart in Figure 3, the unknown quantities in the constructed integral equations are $\bar{E}$ and $\bar{H}$. Since the other field quantities $\bar{J}_{ep}$ and $\bar{J}_{mp}$ or $\bar{D}$ and $\bar{B}$ are linear transforms of $\bar{E}$ and $\bar{H}$, the integral equations can be easily rewritten in a form where the only unknown quantities are $\bar{J}_{ep}$ and $\bar{J}_{mp}$ or $\bar{D}$ and $\bar{B}$ instead.

For a general inhomogeneous bianisotropic body characterized by the constitutive relations (1), we may express $\bar{E}$ and $\bar{H}$ in terms of $\bar{D}$ and $\bar{B}$ as follows

$$\begin{bmatrix} \bar{E} \\ \bar{H} \end{bmatrix} = \begin{bmatrix} \bar{\bar{\alpha}}_1 & \bar{\bar{\alpha}}_2 \\ \bar{\bar{\alpha}}_3 & \bar{\bar{\alpha}}_4 \end{bmatrix} \begin{bmatrix} \bar{D} \\ \bar{B} \end{bmatrix} \tag{26}$$

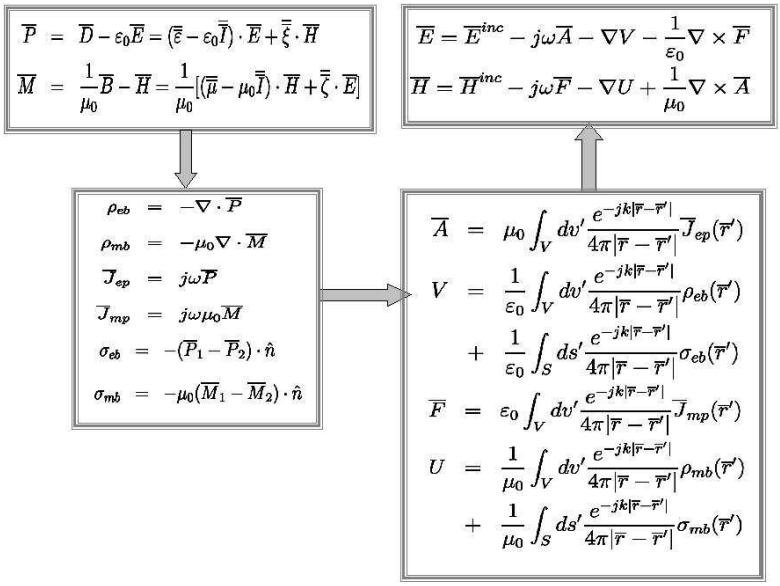

Figure 3. Flow chart of building integral representations.

where $\bar{\bar{\alpha}}_{i=1,2,3,4}$ is given by

$$\begin{bmatrix} \bar{\bar{\alpha}}_1 & \bar{\bar{\alpha}}_2 \\ \bar{\bar{\alpha}}_3 & \bar{\bar{\alpha}}_4 \end{bmatrix} = \begin{bmatrix} \bar{\bar{\varepsilon}} & \bar{\bar{\xi}} \\ \bar{\bar{\zeta}} & \bar{\bar{\mu}} \end{bmatrix}^{-1}. \tag{27}$$

Substituting (26) into (21), we have

$$\begin{aligned} \bar{\bar{\alpha}}_1\bar{D} + \bar{\bar{\alpha}}_2\bar{B} + j\omega\bar{A} + \nabla V + \frac{1}{\varepsilon_0}\nabla\times\bar{F} &= \bar{E}^{inc} \\ \bar{\bar{\alpha}}_3\bar{D} + \bar{\bar{\alpha}}_4\bar{B} + j\omega\bar{F} + \nabla U - \frac{1}{\mu_0}\nabla\times\bar{A} &= \bar{H}^{inc} \end{aligned} \tag{28}$$

where the vector and scalar potentials $\bar{A}$, V, $\bar{F}$, and U can also be written as functions of $\bar{D}$ and $\bar{B}$.

Substituting (26) into (5), we have

$$\begin{bmatrix} \bar{P} \\ \mu_0\bar{M} \end{bmatrix} = \begin{bmatrix} \bar{\bar{\beta}}_1 & \bar{\bar{\beta}}_2 \\ \bar{\bar{\beta}}_3 & \bar{\bar{\beta}}_4 \end{bmatrix} \begin{bmatrix} \bar{D} \\ \bar{B} \end{bmatrix} \tag{29}$$

where

$$\begin{bmatrix} \bar{\bar{\beta}}_1 & \bar{\bar{\beta}}_2 \\ \bar{\bar{\beta}}_3 & \bar{\bar{\beta}}_4 \end{bmatrix} = \begin{bmatrix} \bar{\bar{I}} - \varepsilon_0\bar{\bar{\alpha}}_1 & -\varepsilon_0\bar{\bar{\alpha}}_2 \\ -\mu_0\bar{\bar{\alpha}}_3 & \bar{\bar{I}} - \mu_0\bar{\bar{\alpha}}_4 \end{bmatrix}. \tag{30}$$

Finally, (22)–(25) can be rewritten as functions of $\bar{D}$ and $\bar{B}$ in the following form:

$$\begin{aligned}
\bar{A}(\bar{r}) &= \mu_0 \int_V \bar{J}_{ep}(\bar{r}') G(\bar{r},\bar{r}')\, dv' \\
&= j\omega\mu_0 \int_V \left[\bar{\bar{\beta}}_1(\bar{r}')\, \bar{D}(\bar{r}') + \bar{\bar{\beta}}_2(\bar{r}')\, \bar{B}(\bar{r}')\right] G(\bar{r},\bar{r}')\, dv' \qquad (31) \\
V(\bar{r}) &= \frac{1}{\varepsilon_0}\int_V \rho_{eb}(\bar{r}') G(\bar{r},\bar{r}')\, dv' + \frac{1}{\varepsilon_0}\int_S \sigma_{eb}(\bar{r}') G(\bar{r},\bar{r}')\, ds' \\
&= -\frac{1}{\varepsilon_0}\int_V \nabla'\cdot\left[\bar{\bar{\beta}}_1(\bar{r}')\, \bar{D}(\bar{r}') + \bar{\bar{\beta}}_2(\bar{r}')\, \bar{B}(\bar{r}')\right] G(\bar{r},\bar{r}')\, dv' \\
&\quad + \frac{1}{\varepsilon_0}\int_S \left[\bar{\bar{\beta}}_1(\bar{r}')\, \bar{D}(\bar{r}') + \bar{\bar{\beta}}_2(\bar{r}')\, \bar{B}(\bar{r}')\right]_{of\hat{n}}^{tail}\cdot \hat{n} G(\bar{r},\bar{r}')\, ds' \\
&\quad - \frac{1}{\varepsilon_0}\int_S \left[\bar{\bar{\beta}}_1(\bar{r}')\, \bar{D}(\bar{r}') + \bar{\bar{\beta}}_2(\bar{r}')\, \bar{B}(\bar{r}')\right]_{of\hat{n}}^{head}\cdot \hat{n} G(\bar{r},\bar{r}')\, ds' \qquad (32) \\
\bar{F}(\bar{r}) &= \varepsilon_0 \int_V \bar{J}_{mp}(\bar{r}') G(\bar{r},\bar{r}')\, dv' \\
&= j\omega\varepsilon_0 \int_V \left[\bar{\bar{\beta}}_3(\bar{r}')\, \bar{D}(\bar{r}') + \bar{\bar{\beta}}_4(\bar{r}')\, \bar{B}(\bar{r}')\right] G(\bar{r},\bar{r}')\, dv' \qquad (33) \\
U(\bar{r}) &= \frac{1}{\mu_0}\int_V \rho_{mb}(\bar{r}') G(\bar{r},\bar{r}')\, dv' + \frac{1}{\mu_0}\int_S \sigma_{mb}(\bar{r}') G(\bar{r},\bar{r}')\, ds' \\
&= -\frac{1}{\mu_0}\int_V \nabla'\cdot\left[\bar{\bar{\beta}}_3(\bar{r}')\, \bar{D}(\bar{r}') + \bar{\bar{\beta}}_4(\bar{r}')\, \bar{B}(\bar{r}')\right] G(\bar{r},\bar{r}')\, dv' \\
&\quad + \frac{1}{\mu_0}\int_S \left[\bar{\bar{\beta}}_3(\bar{r}')\, \bar{D}(\bar{r}') + \bar{\bar{\beta}}_4(\bar{r}')\, \bar{B}(\bar{r}')\right]_{of\hat{n}}^{tail}\cdot \hat{n} G(\bar{r},\bar{r}')\, ds' \\
&\quad - \frac{1}{\mu_0}\int_S \left[\bar{\bar{\beta}}_3(\bar{r}')\, \bar{D}(\bar{r}') + \bar{\bar{\beta}}_4(\bar{r}')\, \bar{B}(\bar{r}')\right]_{of\hat{n}}^{head}\cdot \hat{n} G(\bar{r},\bar{r}')\, ds' \qquad (34)
\end{aligned}$$

Substituting (31)–(34) into (28), we obtain a set of integral equations where the only unknowns are $\bar{D}$ and $\bar{B}$.

Following the similar procedure, the integral equations can also be rewritten in a form where the only unknowns are $\bar{J}_{ep}$ and $\bar{J}_{mp}$.

3. SOLUTION USING THE METHOD OF MOMENTS

An inhomogeneous body with an arbitrary 3D shape can be divided into many small cells. If the cell is small enough, the material within the cell can be assumed to be homogeneous. Constitutive properties at the centroid of a cell are assigned to the entire cell. Adjacent cells may possess different constitutive properties to model the inhomogeneity.

As electromagnetic waves propagate through cells, bound charges and polarization currents may exist inside the cells, and bound surface charges may exist on the cell boundaries.

Meshing the body by many little tetrahedra may conform with object surfaces, plus tetrahedra have the least amount of faces and vertices in all 3D objects and the complexity of meshing result is the least among all the methods. For these reasons, although the implementation of tetrahedral mesh is not as straightforward and easy as others, the scatterers in this research were all meshed by tetrahedra.

RWG functions are commonly used basis functions associated with tetrahedral mesh. These functions were first introduced by Rao, Wilton and Glisson as basis functions to represent surface currents in 2D triangle mesh [23]. Later, they extended the concept to 3D tetrahedral meshing and used the RWG basis functions to represent flux densities $\bar{D}$ and $\bar{B}$ [24, 25]. In 3D tetrahedral meshing, each basis function is associated with one face. As shown in Figure 4, for the nth face shared by a pair of tetrahedra, one tetrahedron is noted as T_n^+, and the other one as T_n^-. The fourth point in tetrahedron $T_n^\pm$ which is not on the face n is named as the free vertex of $T_n^\pm$.

The RWG function for the nth face is defined as

$$\begin{aligned}
\bar{f}_n(\bar{r}) &= \bar{f}_n^+(\bar{r}) = +\frac{s_n}{3W_n^+}(\bar{r}-\bar{r}_n^+) = \frac{s_n}{3W_n^+}\bar{\rho}_n^+, \ \forall \bar{r} \in T_n^+ \\
\bar{f}_n(\bar{r}) &= \bar{f}_n^-(\bar{r}) = -\frac{s_n}{3W_n^-}(\bar{r}-\bar{r}_n^-) = \frac{s_n}{3W_n^-}\bar{\rho}_n^-, \ \forall \bar{r} \in T_n^- \\
\bar{f}_n(\bar{r}) &= 0, \qquad \forall \bar{r} \in \text{elsewhere}
\end{aligned} \tag{35}$$

where s_n is the area of the face n. $W_n^\pm$ is the volume of $T_n^\pm$. The vector $\bar{r}$ is the position vector from the origin to the location of the

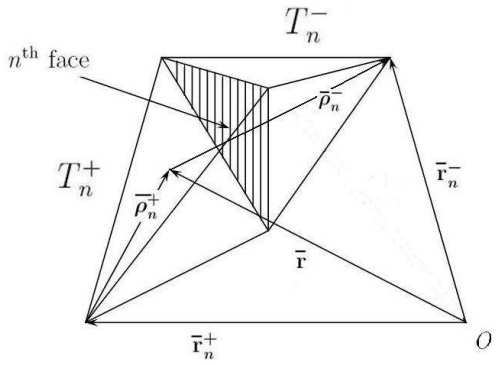

Figure 4. RWG basis function.

field point, and $\bar{r}_n^{\pm}$ is the position vector from the origin to the location of the free vertex in $T_n^{\pm}$. The vector $\bar{\rho}_n^{+}$ is defined as pointing from the free vertex in T_n^{+} to the field point, and $\bar{\rho}_n^{-}$ is defined as the vector pointing from the field point to the free vertex in T_n^{-}.

Each RWG basis function is continuous along the direction which is normal to its associated face inside the scatterer. It is therefore only suitable to use a linear combination of basis functions to approximate those quantities which possess the same property. It is clear that $\bar{E}$ and $\bar{H}$ are not continuous along the direction which is normal to the boundary, hence they cannot be expanded directly by the RWG functions. But it is well known that in a source free region, the electric and magnetic flux densities $\bar{D}$ and $\bar{B}$ are continuous along the direction which is normal to the boundary. If all the unknown quantities in the integral Equations (21) are related to $\bar{D}$ and $\bar{B}$ as shown in (28) instead, a linear combination of RWG basis functions can be applied to expand all the $\bar{D}$ and $\bar{B}$ in (28).

Applying Galerkin's method, and testing Equation (21) with every basis function $\bar{f}_m$, we obtain

$$\begin{aligned} &j\omega < \bar{f}_m, \bar{A}(\bar{r}) > + < \bar{f}_m, \nabla \bar{V}(\bar{r}) > + < \bar{f}_m, \nabla \times \frac{\bar{F}(\bar{r})}{\varepsilon_0} > \\ &+ < \bar{f}_m, \bar{E}(\bar{r}) > = < \bar{f}_m, \bar{E}^{inc}(\bar{r}) > \\ &j\omega < \bar{f}_m, \bar{F}(\bar{r}) > + < \bar{f}_m, \nabla \bar{U}(\bar{r}) > - < \bar{f}_m, \nabla \times \frac{\bar{A}(\bar{r})}{\mu_0} > \\ &+ < \bar{f}_m, \bar{H}(\bar{r}) > = < \bar{f}_m, \bar{H}^{inc}(\bar{r}) > \end{aligned} \tag{36}$$

where the symmetric product of two functions $\bar{f}(\bar{r})$ and $\bar{g}(\bar{r})$ is defined as

$$< \bar{f}(\bar{r}), \bar{g}(\bar{r}) > = \int_V \bar{f}(\bar{r}) \cdot \bar{g}(\bar{r}) d\tau, \tag{37}$$

and domain T is the entire space.

Every term in (36) is expanded in terms of unknown coefficients $\{D_n, B_n, n = 1, 2, \ldots, N\}$. Then (36) is written for each integer value of m from 1 to N. The result is the following matrix equation.

$$\begin{bmatrix} (C_{mn}) & (Y_{mn}) \\ (Z_{mn}) & (A_{mn}) \end{bmatrix} \begin{bmatrix} (D_n) \\ (B_n) \end{bmatrix} = \begin{bmatrix} (E_m) \\ (H_m) \end{bmatrix} \tag{38}$$

where Z_{mn}, A_{mn}, C_{mn}, and Y_{mn} are N by N matrices, and D_n, B_n, E_n and H_n are N dimensional vectors.

The matrix element Z_{mn} is given by

$$\begin{aligned} Z_{mn} = j\omega < \bar{f}_m, \quad \bar{F}(\bar{r}) >_{D_n} + < \bar{f}_m, \quad \nabla U(\bar{r}) >_{D_n} \\ - < \bar{f}_m, \quad \nabla \times \frac{\bar{A}(\bar{r})}{\mu_0} >_{D_n} + < \bar{f}_m, \quad \bar{\bar{\alpha}}_3(\bar{r}) \bar{D}(\bar{r}) >_n \end{aligned} \tag{39}$$

The matrix element A_{mn} is given by

$$A_{mn} = j\omega < \bar{f}_m, \quad \bar{F}(\bar{r}) >_{B_n} + < \bar{f}_m, \quad \nabla U(\bar{r}) >_{B_n} \\ - < \bar{f}_m, \quad \nabla \times \frac{\bar{A}(\bar{r})}{\mu_0} >_{B_n} + < \bar{f}_m, \quad \bar{\bar{\alpha}}_4(\bar{r})\bar{D}(\bar{r}) >_n \tag{40}$$

The matrix element C_{mn} is given by

$$C_{mn} = j\omega < \bar{f}_m, \quad \bar{A}(\bar{r}) >_{D_n} + < \bar{f}_m, \quad \nabla V(\bar{r}) >_{D_n} \\ + < \bar{f}_m, \quad \nabla \times \frac{\bar{F}(\bar{r})}{\varepsilon_0} >_{D_n} + < \bar{f}_m, \quad \bar{\bar{\alpha}}_1(\bar{r})\bar{D}(\bar{r}) >_n \tag{41}$$

The matrix element Y_{mn} is given by

$$Y_{mn} = j\omega < \bar{f}_m, \quad \bar{A}(\bar{r}) >_{B_n} + < \bar{f}_m, \quad \nabla V(\bar{r}) >_{B_n} \\ + < \bar{f}_m, \quad \nabla \times \frac{\bar{F}(\bar{r})}{\varepsilon_0} >_{B_n} + < \bar{f}_m, \quad \bar{\bar{\alpha}}_2(\bar{r})\bar{D}(\bar{r}) >_n \tag{42}$$

where, for the particular value n, $< \bar{f}_m,\ \bar{F}(\bar{r}) >_{D_n}$ is $< \bar{f}_m(\bar{r}),\ \bar{F}(\bar{r}) >$ with $D_n = 1$, $(D_j = 0,\ j = 1, 2, \ldots, N;\ j \neq n)$ and $(B_j = 0,\ j = 1, 2, \ldots, N)$. The quantities $< \bar{f}_m, \nabla U(\bar{r}) >_{D_n}$, $< \bar{f}_m, \nabla \times \frac{\bar{A}(\bar{r})}{\mu_0} >_{D_n}$, and $< \bar{f}_m, \bar{\bar{\alpha}}_3(\bar{r})\bar{D}(\bar{r}) >_n$ are similarly related to $< \bar{f}_m, \nabla U(\bar{r}) >$, $< \bar{f}_m, \nabla \times \frac{\bar{A}(\bar{r})}{\mu_0} >$, and $< \bar{f}_m, \bar{\bar{\alpha}}_3(\bar{r})\bar{D}(\bar{r}) >$, respectively.

The indicated substitutions on their right-hand sides expand (39)–(42) to

$$\begin{aligned} Z_{mn} \ = \ & -\omega^2\varepsilon_0\frac{s_m\bar{\rho}_m^{c+}}{3}\cdot\left[\frac{\bar{\bar{\beta}}_{3n}^{+}s_n}{3}\bar{I}_{1n}^{+}\left(\bar{r}_m^{c+}\right)+\frac{\bar{\bar{\beta}}_{3n}^{-}s_n}{3}\bar{I}_{1n}^{-}\left(\bar{r}_m^{c+}\right)\right] \\ & -\omega^2\varepsilon_0\frac{s_m\bar{\rho}_m^{c-}}{3}\cdot\left[\frac{\bar{\bar{\beta}}_{3n}^{+}s_n}{3}\bar{I}_{1n}^{+}\left(\bar{r}_m^{c-}\right)+\frac{\bar{\bar{\beta}}_{3n}^{-}s_n}{3}\bar{I}_{1n}^{-}\left(\bar{r}_m^{c-}\right)\right] \\ & +\frac{s_m}{\mu_0}\Bigg[I_{sn}^{+}\left(\bar{\bar{\beta}}_{3n}^{+},\bar{r}_m^{c-}\right)-I_{sn}^{-}\left(\bar{\bar{\beta}}_{3n}^{-},\bar{r}_m^{c-}\right) \\ & -Tr\left(\bar{\bar{\beta}}_{3n}^{+}\right)\frac{s_n}{3}I_{2n}^{+}\left(r_m^{c-}\right)+Tr\left(\bar{\bar{\beta}}_{3n}^{-}\right)\frac{s_n}{3}I_{2n}^{-}\left(r_m^{c-}\right) \\ & -I_{sn}^{+}\left(\bar{\bar{\beta}}_{3n}^{+},\bar{r}_m^{c+}\right)+I_{sn}^{-}\left(\bar{\bar{\beta}}_{3n}^{-},\bar{r}_m^{c+}\right) \\ & +Tr\left(\bar{\bar{\beta}}_{3n}^{+}\right)\frac{s_n}{3}I_{2n}^{+}\left(r_m^{c+}\right)-Tr\left(\bar{\bar{\beta}}_{3n}^{-}\right)\frac{s_n}{3}I_{2n}^{-}\left(r_m^{c+}\right)\Bigg] \end{aligned}$$

$$
\begin{aligned}
&-j\omega\cdot\left[\frac{s_n}{3}I_{3n}^{+}\left(\bar{\bar{\beta}}_{1n}^{+},T_m^{+}\right)+\frac{s_n}{3}I_{3n}^{-}\left(\bar{\bar{\beta}}_{1n}^{-},T_m^{+}\right)\right]\\
&-j\omega\cdot\left[\frac{s_n}{3}I_{3n}^{+}\left(\bar{\bar{\beta}}_{1n}^{+},T_m^{-}\right)+\frac{s_n}{3}I_{3n}^{-}\left(\bar{\bar{\beta}}_{1n}^{-},T_m^{-}\right)\right]\\
&+\left[I_{mn}^{+}\left(\bar{\bar{\alpha}}_{3m}^{+}\right)+I_{mn}^{-}\left(\bar{\bar{\alpha}}_{3m}^{-}\right)\right] \qquad (43)
\end{aligned}
$$

$$
\begin{aligned}
A_{mn} \;=\; & -\omega^2\varepsilon_0\frac{s_m\bar{\rho}_m^{c+}}{3}\cdot\left[\frac{\bar{\bar{\beta}}_{4n}^{+}s_n}{3}\bar{I}_{1n}^{+}\left(\bar{r}_m^{c+}\right)+\frac{\bar{\bar{\beta}}_{4n}^{-}s_n}{3}\bar{I}_{1n}^{-}\left(\bar{r}_m^{c+}\right)\right]\\
&-\omega^2\varepsilon_0\frac{s_m\bar{\rho}_m^{c-}}{3}\cdot\left[\frac{\bar{\bar{\beta}}_{4n}^{+}s_n}{3}\bar{I}_{1n}^{+}\left(\bar{r}_m^{c-}\right)+\frac{\bar{\bar{\beta}}_{4n}^{-}s_n}{3}\bar{I}_{1n}^{-}\left(\bar{r}_m^{c-}\right)\right]\\
&+\frac{s_m}{\mu_0}\left[I_{sn}^{+}\left(\bar{\bar{\beta}}_{4n}^{+},\bar{r}_m^{c-}\right)-I_{sn}^{-}\left(\bar{\bar{\beta}}_{4n}^{-},\bar{r}_m^{c-}\right)\right.\\
&-Tr\left(\bar{\bar{\beta}}_{4n}^{+}\right)\frac{s_n}{3}I_{2n}^{+}\left(r_m^{c-}\right)+Tr\left(\bar{\bar{\beta}}_{4n}^{-}\right)\frac{s_n}{3}I_{2n}^{-}\left(r_m^{c-}\right)\\
&-I_{sn}^{+}\left(\bar{\bar{\beta}}_{4n}^{+},\bar{r}_m^{c+}\right)+I_{sn}^{-}\left(\bar{\bar{\beta}}_{4n}^{-},\bar{r}_m^{c+}\right)\\
&\left.+Tr\left(\bar{\bar{\beta}}_{4n}^{+}\right)\frac{s_n}{3}I_{2n}^{+}\left(r_m^{c+}\right)-Tr\left(\bar{\bar{\beta}}_{4n}^{-}\right)\frac{s_n}{3}I_{2n}^{-}\left(r_m^{c+}\right)\right]\\
&-j\omega\cdot\left[\frac{s_n}{3}I_{3n}^{+}\left(\bar{\bar{\beta}}_{2n}^{+},T_m^{+}\right)+\frac{s_n}{3}I_{3n}^{-}\left(\bar{\bar{\beta}}_{2n}^{-},T_m^{+}\right)\right]\\
&-j\omega\cdot\left[\frac{s_n}{3}I_{3n}^{+}\left(\bar{\bar{\beta}}_{2n}^{+},T_m^{-}\right)+\frac{s_n}{3}I_{3n}^{-}\left(\bar{\bar{\beta}}_{2n}^{-},T_m^{-}\right)\right]\\
&+\left[I_{mn}^{+}\left(\bar{\bar{\alpha}}_{4m}^{+}\right)+I_{mn}^{-}\left(\bar{\bar{\alpha}}_{4m}^{-}\right)\right] \qquad (44)
\end{aligned}
$$

$$
\begin{aligned}
C_{mn} \;=\; & -\omega^2\mu_0\frac{s_m\bar{\rho}_m^{c+}}{3}\cdot\left[\frac{\bar{\bar{\beta}}_{1n}^{+}s_n}{3}\bar{I}_{1n}^{+}\left(\bar{r}_m^{c+}\right)+\frac{\bar{\bar{\beta}}_{1n}^{-}s_n}{3}\bar{I}_{1n}^{-}\left(\bar{r}_m^{c+}\right)\right]\\
&-\omega^2\mu_0\frac{s_m\bar{\rho}_m^{c-}}{3}\cdot\left[\frac{\bar{\bar{\beta}}_{1n}^{+}s_n}{3}\bar{I}_{1n}^{+}\left(\bar{r}_m^{c-}\right)+\frac{\bar{\bar{\beta}}_{1n}^{-}s_n}{3}\bar{I}_{1n}^{-}\left(\bar{r}_m^{c-}\right)\right]\\
&+\frac{s_m}{\varepsilon_0}\left[I_{sn}^{+}\left(\bar{\bar{\beta}}_{1n}^{+},\bar{r}_m^{c-}\right)-I_{sn}^{-}\left(\bar{\bar{\beta}}_{1n}^{-},\bar{r}_m^{c-}\right)\right.
\end{aligned}
$$

$$
\begin{aligned}
&-Tr\left(\bar{\bar{\beta}}_{1n}^{+}\right)\frac{s_n}{3}I_{2n}^{+}\left(r_m^{c-}\right)+Tr\left(\bar{\bar{\beta}}_{1n}^{-}\right)\frac{s_n}{3}I_{2n}^{-}\left(r_m^{c-}\right)\\
&-I_{sn}^{+}\left(\bar{\bar{\beta}}_{1n}^{+},\bar{r}_m^{c+}\right)+I_{sn}^{-}\left(\bar{\bar{\beta}}_{1n}^{-},\bar{r}_m^{c+}\right)+Tr\left(\bar{\bar{\beta}}_{1n}^{+}\right)\frac{s_n}{3}I_{2n}^{+}\left(r_m^{c+}\right)\\
&-Tr\left(\bar{\bar{\beta}}_{1n}^{-}\right)\frac{s_n}{3}I_{2n}^{-}\left(r_m^{c+}\right)\Bigg]\\
&+j\omega\cdot\left[\frac{s_n}{3}I_{3n}^{+}\left(\bar{\bar{\beta}}_{3n}^{+},T_m^{+}\right)+\frac{s_n}{3}I_{3n}^{-}\left(\bar{\bar{\beta}}_{3n}^{-},T_m^{+}\right)\right]\\
&+j\omega\cdot\left[\frac{s_n}{3}I_{3n}^{+}\left(\bar{\bar{\beta}}_{3n}^{+},T_m^{-}\right)+\frac{s_n}{3}I_{3n}^{-}\left(\bar{\bar{\beta}}_{3n}^{-},T_m^{-}\right)\right]\\
&+\left[I_{mn}^{+}\left(\bar{\bar{\alpha}}_{1m}^{+}\right)+I_{mn}^{-}\left(\bar{\bar{\alpha}}_{1m}^{-}\right)\right]
\end{aligned}
\tag{45}
$$

$$
\begin{aligned}
Y_{mn} \;=\; & -\omega^2\mu_0\frac{s_m\bar{\rho}_m^{c+}}{3}\cdot\left[\frac{\bar{\bar{\beta}}_{2n}^{+}s_n}{3}\bar{I}_{1n}^{+}\left(\bar{r}_m^{c+}\right)+\frac{\bar{\bar{\beta}}_{2n}^{-}s_n}{3}\bar{I}_{1n}^{-}\left(\bar{r}_m^{c+}\right)\right]\\
&-\omega^2\mu_0\frac{s_m\bar{\rho}_m^{c-}}{3}\cdot\left[\frac{\bar{\bar{\beta}}_{2n}^{+}s_n}{3}\bar{I}_{1n}^{+}\left(\bar{r}_m^{c-}\right)+\frac{\bar{\bar{\beta}}_{2n}^{-}s_n}{3}\bar{I}_{1n}^{-}\left(\bar{r}_m^{c-}\right)\right]\\
&+\frac{s_m}{\varepsilon_0}\Bigg[I_{sn}^{+}\left(\bar{\bar{\beta}}_{2n}^{+},\bar{r}_m^{c-}\right)-I_{sn}^{-}\left(\bar{\bar{\beta}}_{2n}^{-},\bar{r}_m^{c-}\right)\\
&-Tr\left(\bar{\bar{\beta}}_{2n}^{+}\right)\frac{s_n}{3}I_{2n}^{+}\left(r_m^{c-}\right)+Tr\left(\bar{\bar{\beta}}_{2n}^{-}\right)\frac{s_n}{3}I_{2n}^{-}\left(r_m^{c-}\right)\\
&-I_{sn}^{+}\left(\bar{\bar{\beta}}_{2n}^{+},\bar{r}_m^{c+}\right)+I_{sn}^{-}\left(\bar{\bar{\beta}}_{2n}^{-},\bar{r}_m^{c+}\right)\\
&+Tr\left(\bar{\bar{\beta}}_{2n}^{+}\right)\frac{s_n}{3}I_{2n}^{+}\left(r_m^{c+}\right)-Tr\left(\bar{\bar{\beta}}_{2n}^{-}\right)\frac{s_n}{3}I_{2n}^{-}\left(r_m^{c+}\right)\Bigg]\\
&+j\omega\cdot\left[\frac{s_n}{3}I_{3n}^{+}\left(\bar{\bar{\beta}}_{4n}^{+},T_m^{+}\right)+\frac{s_n}{3}I_{3n}^{-}\left(\bar{\bar{\beta}}_{4n}^{-},T_m^{+}\right)\right]\\
&+j\omega\cdot\left[\frac{s_n}{3}I_{3n}^{+}\left(\bar{\bar{\beta}}_{4n}^{+},T_m^{-}\right)+\frac{s_n}{3}I_{3n}^{-}\left(\bar{\bar{\beta}}_{4n}^{-},T_m^{-}\right)\right]\\
&+\left[I_{mn}^{+}\left(\bar{\bar{\alpha}}_{2m}^{+}\right)+I_{mn}^{-}\left(\bar{\bar{\alpha}}_{2m}^{-}\right)\right].
\end{aligned}
\tag{46}
$$

where

$$\bar{I}_{1n}^{\pm}(\bar{r}) = \frac{1}{W_n^{\pm}} \int_{T_n^{\pm}} \bar{\rho}_n^{'\pm} G(\bar{r}, \bar{r}')\, d\tau', \tag{47}$$

$$I_{2n}^{\pm}(\bar{r}) = \frac{1}{W_n^{\pm}} \int_{T_n^{\pm}} G(\bar{r}, \bar{r}')\, d\tau' \tag{48}$$

$$I_{mn}^{\pm}(\bar{\bar{\alpha}}) = \int_{T_m^{\pm}} \bar{f}_m(\bar{r}) \cdot \bar{\bar{\alpha}} \bar{f}_n(\bar{r})\, d\tau. \tag{49}$$

Integral $I_{3n}^{\pm}(\bar{\bar{\beta}}, T_m^{\pm})$ is evaluated as follows

$$\begin{aligned} I_{3n}^{\pm}\left(\bar{\bar{\beta}}, T_m^{+}\right) &= -\frac{s_m}{3W_m^{+}} \sum_{i=1}^{4} s_{T_m^{+},i} \bar{\bar{\beta}} \bar{I}_{1n}^{\pm}\left(\bar{r}_{T_m^{+},i}^{c}\right) \cdot \left[\hat{n}_{T_m^{+},i} \times \left(\bar{r}_{T_m^{+},i}^{c} - \bar{r}_m^{+}\right)\right] \\ I_{3n}^{\pm}\left(\bar{\bar{\beta}}, T_m^{-}\right) &= -\frac{s_m}{3W_m^{-}} \sum_{i=1}^{4} s_{T_m^{-},i} \bar{\bar{\beta}} \bar{I}_{1n}^{\pm}\left(\bar{r}_{T_m^{-},i}^{c}\right) \cdot \left[\hat{n}_{T_m^{-},i} \times \left(\bar{r}_{T_m^{-},i}^{c} - \bar{r}_m^{-}\right)\right] \end{aligned} \tag{50}$$

where $\bar{\bar{\beta}}$ is a tensor, $S_{T_m^{\pm},i}$, $i = 1, 2, 3, 4$ represents the ith faces of tetrahedron $T_m^{\pm}$, and $\hat{n}_{T_m^{\pm},i}$ is a unit vector in a direction which is normal to the ith face of tetrahedron $T_m^{\pm}$. $\hat{n}_{T_m^{+},i}$ points toward the outside of tetrahedron T_m^{+} and $\hat{n}_{T_m^{-},i}$ points toward the inside of tetrahedron T_m^{-}.

Integral $I_{sn}^{\pm}(\bar{\bar{\beta}}, \bar{r})$ is evaluated as follows

$$I_{sn}^{\pm}\left(\bar{\bar{\beta}}, \bar{r}\right) = \frac{s_n}{3W_n^{\pm}} \sum_{i=1}^{4} \left[\bar{\bar{\beta}} \int_{S_{T_n^{\pm},i}} \bar{\rho}_n^{'\pm} G(\bar{r}, \bar{r}')\, ds'\right] \cdot \hat{n}_{T_n^{\pm},i}. \tag{51}$$

Here, $\bar{\bar{\beta}}$ is a tensor. $S_{T_n^{\pm},i}$, $i = 1, 2, 3, 4$ is the ith face of the tetrahedron $T_n^{\pm}$, and $\hat{n}_{T_n^{\pm},i}$ is a unit vector in the direction that is normal to the face $S_{T_n^{\pm},i}$, pointing from the tetrahedron T_n^{+} to the tetrahedron T_n^{-}.

Finally, $Tr(\bar{\bar{\beta}})$ is the trace of the tensor $\bar{\bar{\beta}}$, defined as the summation of the diagonal elements of $\bar{\bar{\beta}}$.

While developing a solution to the problem of interest, a special care has been taken to the evaluation of the corresponding integrals presented above. For example, certain volume and surface integrals become singular when evaluated at the centroids of meshing cells. In such cases, analytical methods introduced by Wilton, et al. in [25] can be used to evaluate these singular integrals.

4. NUMERICAL RESULTS

A MATLAB program is developed to set up the MoM matrix equation, and by solving the MoM matrix equation, the electromagnetic fields inside the scatterer are obtained. Bound charge distribution, polarization current distribution, and the fields outside the scatterer are all calculated from the internal fields. The bistatic radar cross section (RCS), an important property of a scattering object, is also calculated from the internal fields. In this section electromagnetic scattering problems involving various materials and geometries are solved by the MATLAB program that we developed. These electromagnetic scattering problems were also studied and solved previously by other researchers using different methods. The numerical results obtained by using the method presented in this paper are then compared with the solutions obtained previously by other researchers to validate the theoretic formulations and implementation of the computer program. It also shows that the method presented in this paper is general enough to handle various cases which had to be solved by different methods previously.

A case of electromagnetic scattering by a homogeneous dielectric sphere is first considered and the results are compared with the solutions obtained by Demir's scattering field solver [13] and with the work of Schaubert et al. in [24]. An inhomogeneous dielectric sphere scattering problem is also solved and checked with the results of Carvalho et al. in [26]. The more complicated case of a magnetic and dielectric sphere is analyzed to compare with the solution obtained by Demir's solver [13]. The cases involving a homogeneous or inhomogeneous chiral sphere are solved to compare with results in Worasawate's dissertation [27] and Hasanovic's dissertation [28]. Gyroelectric and gyromagnetic sphere cases are investigated and checked with results of Geng and Zhu in their work [29–31] and Yagli's dissertation [17]. The results of scattering from chiral materials in cubical and cylindrical geometries are also checked with [28]. Here we present only three cases for validation of our results.

Copolarized and cross-polarized bistatic radar cross sections $\sigma_{\theta\theta}$ of $\phi = 0^\circ$ and $\sigma_{\phi\theta}$ of $\phi = 90^\circ$ are shown in Figure 6 for a two-layered dielectric sphere shown in Figure 5. The sphere is of radius $R = r_2$ and contains two layers of dielectric material of different permittivities. The inner sphere has a radius $r_1 = 0.5r_2$ and has the relative permittivity $\varepsilon_{r1} = 4$ while the outside layer has the relative permittivity $\varepsilon_{r2} = 9$. The sphere is illuminated by a plane electromagnetic wave propagating in the z direction, which has its electric field in the x direction, i.e., $\bar{E}^{inc} = \hat{x}E^{inc}e^{-jk_0z}$ and $\bar{H}^{inc} = \hat{y}H^{inc}e^{-jk_0z}$ where $E^{inc} = 377$ [V/m].

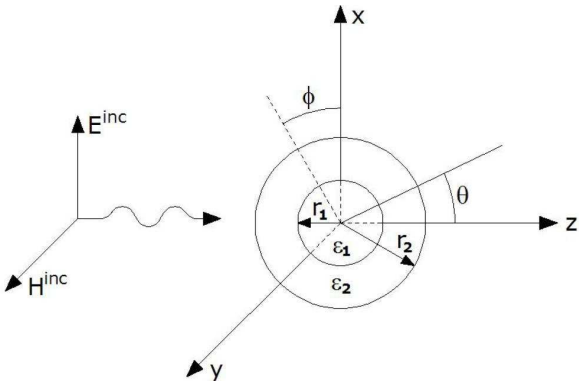

Figure 5. Two-layered dielectric sphere, $k_0 r_2 = 0.408$, $r_2/r_1 = 2$, $\varepsilon_{r1} = 4$, $\varepsilon_{r2} = 9$.

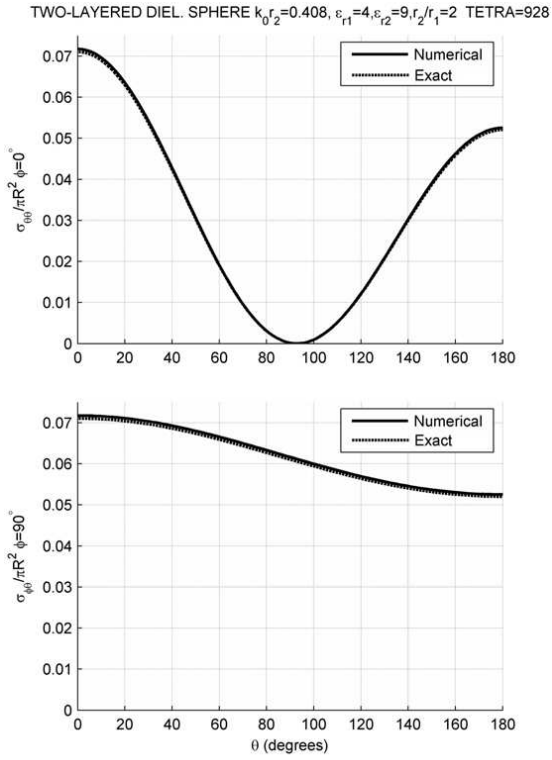

Figure 6. Bistatic radar cross sections $\sigma_{\theta\theta}$ and $\sigma_{\phi\theta}$ of a two-layered dielectric sphere, $k_0 r_2 = 0.408$, $r_2/r_1 = 2$, $\varepsilon_{r1} = 4$, $\varepsilon_{r2} = 9$.

Carvalho and Mendes solved the same problem in their work [26] with the use of the method of moments and 3-D solenoidal basis functions. The exact RCS results using the method of Mie's series expansion is presented in [26] as comparison. A good agreement can be observed between our numerical result and the exact solutions.

To further validate the proposed method, a finite circular chiral cylinder shown in Figure 7 has been illuminated by a plane electromagnetic wave and investigated as a scatterer. The radius R of the cylinder is so chosen that $k_0R = 1.5$ and the height of the cylinder is $h = 0.35\lambda_0$ where $\lambda_0 = 2\pi/k_0$ and k_0 is the wavenumber in free space.

Copolarized and cross-polarized bistatic radar cross sections $\sigma_{\theta\theta}$ of $\phi = 0^\circ$ and $\sigma_{\phi\theta}$ of $\phi = 0^\circ$ are shown in Figure 8. The numerical results are compared with the results shown in [27] and [28] and a good agreement is observed.

As a third example, we present the results of scattering by a homogeneous gyroelectric sphere shown in Figure 9. The sphere is of radius R and has the relative permittivity tensor $\bar{\bar{\varepsilon}}_r = \begin{bmatrix} 5 & j & 0 \\ -j & 5 & 0 \\ 0 & 0 & 7 \end{bmatrix}$ and relative permeability $\mu_r = 1$.

The sphere is illuminated by a plane electromagnetic wave propagating in the z direction, which has its electric field in the x direction, i.e., $\bar{E}^{inc} = \hat{x}E^{inc}e^{-jk_0z}$ and $\bar{H}^{inc} = \hat{y}H^{inc}e^{-jk_0z}$ where $E^{inc} = 1$[V/m].

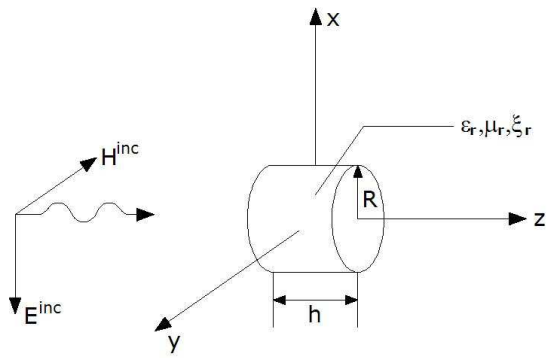

Figure 7. Chiral cylinder illuminated by a plane EM wave, $k_0R = 1.5$, $h = 0.35\lambda$, $\epsilon_r = 2$, $\mu_r = 1$, and $\xi_r = 0.3$.

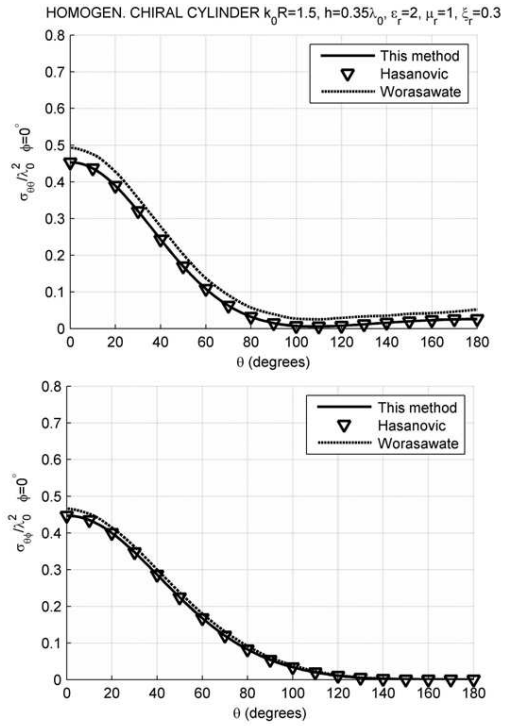

Figure 8. Bistatic radar cross sections $\sigma_{\theta\theta}$ and $\sigma_{\theta\phi}$ of a chiral cylinder illuminated by a plane EM wave, $k_0R = 1.5$, $h = 0.35\lambda$, $\epsilon_r = 2$, $\mu_r = 1$, and $\xi_r = 0.3$.

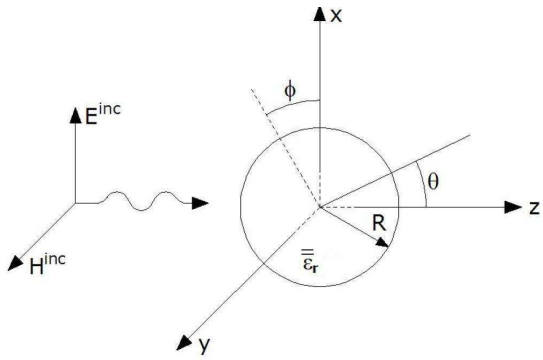

Figure 9. Gyroelectric sphere illuminated by a plane EM wave, $k_0R = 0.5$, $\varepsilon_{r_{xx}} = \varepsilon_{r_{yy}} = 5$, $\varepsilon_{r_{zz}} = 7$, $\varepsilon_{r_{xy}} = -\varepsilon_{r_{yx}} = j$, $\mu_r = 1$.

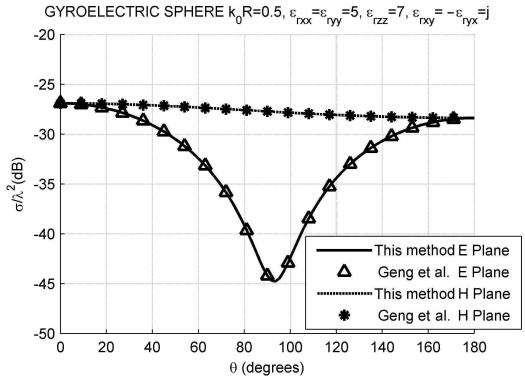

Figure 10. Bistatic radar cross section of a gyroelectric sphere illuminated by a plane EM wave, $k_0R = 0.5$, $\varepsilon_{r_{xx}} = \varepsilon_{r_{yy}} = 5$, $\varepsilon_{r_{zz}} = 7$, $\varepsilon_{r_{xy}} = -\varepsilon_{r_{yx}} = j$, $\mu_r = 1$.

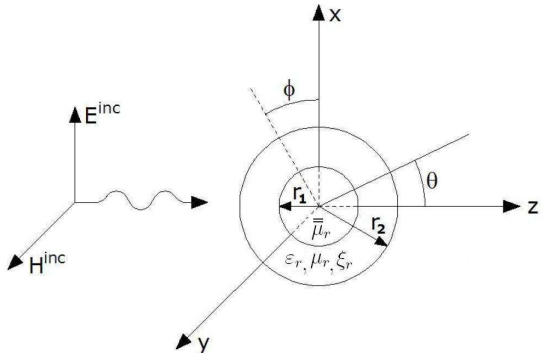

Figure 11. A two-layered dispersive chiroferrite sphere illuminated by a plane EM wave, for $r_2 = 7.2\,\text{cm}$, and $r_1 = 0.5r_2$ at the frequencies of 0.4 GHz, 0.6 GHz, 1 GHz, and 1.2 GHz ($\alpha = 0.1$, $\omega_0 = 2\pi \times 2 \times 10^9$, $\omega_m = 2\pi \times 2 \times 10^9$, $\varepsilon_{\infty r} = 2$, $\varepsilon_{sr} = 5$, $\omega_\varepsilon = 2\pi \times 2 \times 10^9$, $\xi_\varepsilon = 0.5$, $\mu_{\infty r} = 1.1$, $\mu_{sr} = 1.8$, $\omega_\mu = 2\pi \times 2 \times 10^9$, $\xi_\mu = 0.5$, $\tau_\kappa = \frac{0.5}{\omega_\kappa}$, $\omega_\kappa = 2\pi \times 2 \times 10^9$, $\xi_\kappa = 0.3$).

Corresponding tensors $\bar{\bar{\varepsilon}} = \varepsilon_0 \begin{bmatrix} \varepsilon_{r_{xx}} & \varepsilon_{r_{xy}} & 0 \\ \varepsilon_{r_{yx}} & \varepsilon_{r_{yy}} & 0 \\ 0 & 0 & \varepsilon_{rzz} \end{bmatrix}$, $\bar{\bar{\mu}} = \begin{bmatrix} \mu_0\mu_r & 0 & 0 \\ 0 & \mu_0\mu_r & 0 \\ 0 & 0 & \mu_0\mu_r \end{bmatrix}$, $\bar{\bar{\xi}} = \begin{bmatrix} 0 & 0 & 0 \\ 0 & 0 & 0 \\ 0 & 0 & 0 \end{bmatrix}$ and $\bar{\bar{\zeta}} = \begin{bmatrix} 0 & 0 & 0 \\ 0 & 0 & 0 \\ 0 & 0 & 0 \end{bmatrix}$ are assigned.

The numerical results obtained from this method are presented here. Total bistatic radar cross section σ is shown in Figure 10. The RCS results are compared with Geng and Zhu's work in [29] and [30] using the MoM-CGM-FFT method. The same problem is also solved in Yagli's dissertation [17] using the TLM method. Good agreement in RCS results is observed for these different methods.

This section presents the results of scattering from a two-layered dispersive chiroferrite sphere shown in Figure 11. The sphere is of radius $R = r_2 = 7.2\,\text{cm}$ and contains two layers. The radius of the inner sphere is r_1. The outside layer and the inner sphere are made of a dispersive chiral material and a dispersive ferrite material, respectively. These two materials are described below.

When biased by a DC magnetic field $\bar{B}_0 = \hat{a}_z B_0$, ferrite materials, whose permittivity tensor is $\bar{\bar{\varepsilon}} = \varepsilon_0 \bar{\bar{I}}$, are characterized by their permeability tensors $\bar{\bar{\mu}} = \mu_0 \bar{\bar{\mu}}_r$ where

$$\bar{\bar{\mu}}_r = \begin{bmatrix} \mu_1 & j\mu_2 & 0 \\ -j\mu_2 & \mu_1 & 0 \\ 0 & 0 & \mu_3 \end{bmatrix}. \tag{52}$$

The elements in the permeability tensor are formulated as [17]

$$\begin{aligned} \mu_1 &= 1 + \frac{(\omega_0 + j\omega\alpha)\omega_m}{(\omega_0 + j\omega\alpha)^2 - \omega^2} \\ \mu_2 &= \frac{\omega\omega_m}{(\omega_0 + j\omega\alpha)^2 - \omega^2} \\ \mu_3 &= 1 \end{aligned} \tag{53}$$

where α is the ferrite damping factor, ω_0 is the Larmor precession frequency and ω_m is the saturation magnetization frequency.

The Larmor precession frequency ω_0 and the saturation magnetization frequency ω_m are determined by the DC magnetic field bias by [17]

$$\begin{aligned} \omega_0 &= \gamma_m H_0 \\ \omega_m &= \gamma_m M_0. \end{aligned} \tag{54}$$

where γ_m is the gyromagnetic ratio, H_0 the magnitude of the applied DC magnetic field, and M_0 the magnitude of saturated magnetization vector. $\bar{M}_0$ is in the same direction of the applied magnetic field $\bar{H}_0$.

Once the Larmor precession frequency, saturation magnetization frequency, and ferrite damping factor are given, the permeability tensor $\bar{\bar{\mu}}$ can be evaluated at any frequency.

The constitutive equations for dispersive chiral media can be written as

$$\begin{aligned} \bar{D}(\omega) &= \varepsilon(\omega)\bar{E}(\omega) - j\kappa(\omega)\sqrt{\varepsilon_0\mu_0}\bar{H}(\omega) \\ \bar{B}(\omega) &= \mu(\omega)\bar{H}(\omega) + j\kappa(\omega)\sqrt{\varepsilon_0\mu_0}\bar{E}(\omega) \end{aligned} \tag{55}$$

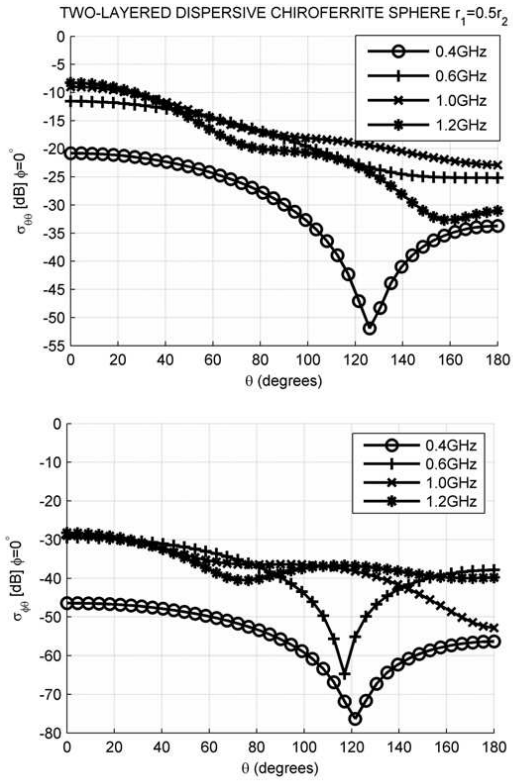

Figure 12. Bistatic radar cross sections $\sigma_{\theta\theta}$ and $\sigma_{\phi\theta}$ of a two-layered dispersive chiroferrite sphere illuminated by a plane EM wave, for $r_2 = 7.2\,\text{cm}$, and $r_1 = 0.5r_2$ at the frequencies of 0.4 GHz, 0.6 GHz, 1 GHz, and 1.2 GHz ($\alpha = 0.1,\ \omega_0 = 2\pi \times 2 \times 10^9,\ \omega_m = 2\pi \times 2 \times 10^9,\ \varepsilon_{\infty r} = 2,\ \varepsilon_{sr} = 5,\ \omega_\varepsilon = 2\pi \times 2 \times 10^9,\ \xi_\varepsilon = 0.5,\ \mu_{\infty r} = 1.1,\ \mu_{sr} = 1.8,\ \omega_\mu = 2\pi \times 2 \times 10^9,\ \xi_\mu = 0.5,\ \tau_\kappa = \frac{0.5}{\omega_\kappa},\ \omega_\kappa = 2\pi \times 2 \times 10^9,\ \xi_\kappa = 0.3$).

In most of the cases, the Lorentz model is used to characterize the dispersive nature of permittivity and permeablity. The Condon model is generally used to describe the dispersive nature of chirality [18]. The Lorentz model is in the form

$$\begin{aligned} \varepsilon(\omega) &= \varepsilon_\infty + \frac{(\varepsilon_s - \varepsilon_\infty)\omega_\varepsilon^2}{\omega_\varepsilon^2 - \omega^2 + j2\omega_\varepsilon\xi_\varepsilon\omega} \\ \mu(\omega) &= \mu_\infty + \frac{(\mu_s - \mu_\infty)\omega_\mu^2}{\omega_\mu^2 - \omega^2 + j2\omega_\mu\xi_\mu\omega}. \end{aligned} \tag{56}$$

The Condon model is in the form

$$\kappa(\omega) = \frac{\tau_\kappa \omega_\kappa^2 \omega}{\omega_\kappa^2 - \omega^2 + j2\omega_\kappa \xi_\kappa \omega}. \tag{57}$$

We solved the two cases of $r_1 = 0.5r_2$, and $r_1 = 0.3r_2$. For comparison, letting $r_1 = 0$, the results of scattering from a homogeneous dispersive chiral sphere of radius $R = r_2 = 7.2\,\text{cm}$ are also presented here.

The sphere is illuminated by a plane electromagnetic wave propagating in the z direction, which has its electric field in the x direction, i.e., $\bar{E}^{inc} = \hat{x}E^{inc}e^{-jk_0z}$ and $\bar{H}^{inc} = \hat{y}H^{inc}e^{-jk_0z}$ where $E^{inc} = 1[\text{V/m}]$, as shown in Figure 11.

The numerical results are obtained at the frequencies of 0.4 GHz, 0.6 GHz, 1 GHz, and 1.2 GHz. The corresponding values of k_0R are 0.6032, 0.9048, 1.508, and 1.809, respectively. Figure 12 shows the copolarized and cross-polarized bistatic radar cross sections $\sigma_{\theta\theta}$ of $\phi = 0^\circ$ and $\sigma_{\phi\theta}$ of $\phi = 0^\circ$ when the inner sphere radius $r_1 = 0.5r_2$.

5. CONCLUDING REMARKS

This paper presents a general numerical solution based on the method of moments (MoM) for various electromagnetic scattering problems. The scatterer is assumed to be the most general case of a linear and stationary material: an inhomogeneous bianisotropic medium of an arbitrarily shaped three-dimensional geometry. It is the main contribution of this paper that the applications of the MoM are extended to solve scattering problems involving such a complicated medium. The method is implemented in a MATLAB program. A general-purpose electromagnetic scattering field solver that could handle all kinds of inhomogeneities, dispersion, anisotropy, chirality, and bianisotropy is offered to the electromagnetic community. To the best of the authors' knowledge, this is the first scattering field solver that is able to cover such a wide range. The flexibility of the method makes it very suitable to be applied to analyze electromagnetic field interactions with all kinds of novel materials offered by the fast evolving material technology.

The method applies the volume equivalence principle by which the bounded charges and polarization currents in the body are modeled as the sources of the scattered fields. Comparing with the surface equivalence principle where only equivalent surface currents are placed at the boundaries and inhomogeneities are difficult to handle, the present method is not hampered by inhomogeneities and obtains a more accurate field solution inside the body. The assumption of bound charges and polarization currents distributed in the body makes it easy to solve problems involving inhomogeneous scatterers.

The problem is described by a set of mixed potential formulations, where the total fields are separated into the incident fields and the scattered fields, and the scattered fields are related to the electric and magnetic potentials which are excited by electric and magnetic bound charges and polarization currents. The potentials are further related to the electric and magnetic polarizations and finally are formulated as the functions of the total fields. Thus, the electric and magnetic field integral equations are constructed.

The electric and magnetic field integral equations cannot be solved analytically. The method of moments (MoM) technique is applied to obtain a numerical solution of the integral equations. First, the inhomogeneous scattering problem is modeled by dividing the scatterer body into many small tetrahedral cells; within a cell the material is assumed to be homogeneous and approximated by the properties at the centroid of the tetrahedron. A set of face-based functions, RWG basis functions, are introduced so that the unknown quantities in the integral equations are expanded in terms of these basis functions. Galerkin's testing method is used to transform the original integral equations to a MoM matrix equation. The MoM matrix equation can easily be solved to determine the original unknown quantities. Thus, a numerical solution of the original integral equations is obtained.

The proposed formulation is evaluated and verified through examples of scattering by various scatterers illuminated by an electromagnetic plane wave. Numerical results of these scattering problems are presented and compared with results obtained using other methods. A good agreement is observed. Thus, the method in this paper is validated and its accuracy is confirmed.

After its verification, the proposed method has been applied to the problem of a scattering by a two-layered dispersive chiroferrite sphere. This problem is general enough and has not been solved in the past. All the presented numerical cases prove that the method in this paper is general enough to solve various problems which had to be solved by different methods previously.

As mentioned earlier, the MoM technique that uses the volume equivalence principle has many advantages over the surface approach, especially because it may be applied with better accuracy to inhomogeneous scatterers. However, it may suffer from a rapid growth of computational complexity with increased mesh resolution in the case of electrically large objects. The following improvements can be done in the future to increase the mesh size limit and reduce the simulation time. First, rewriting the algorithm in a compiled computer language such as C and Fortran which are much faster than the interpreted language MATLAB will significantly reduce the computation time.

Secondly, carefully controlling the meshing process will further reduce the mesh complexity. If the mesh is dense at the locations where the fields vary rapidly over the distance, and less dense at the locations where field variation is more steady, the same level of accuracy can be achieved with less complexity. In the current code, the meshing process is a knowledge based process and the mesh is refined at the boundaries where the field variation is predicted to be significant. It would be helpful if the meshing process is realized automatically so that the program is able to handle more complicated structures. It would be even better if an adaptive meshing method can be adopted. Using such a method, a problem is solved initially with a coarse mesh, and the refinements are added based on the previous solution and are concentrated in the locations where fields change rapidly and where refinements are necessary. Other acceleration techniques such as those based on the fast Fourier transform [32] can also be applied in further research with the objective of increasing the efficiency of the computer program through a reduction of memory and time requirements.

Once the cells of a mesh are numbered further reduction of the number of the unknowns in the MoM matrix equation can be done by experimenting with another set of basis functions. The number of the face-based RWG functions used in our formulation is equal to the number of the faces in the mesh. We also know that the number of faces in a volume mesh is considerably larger than the number of the edges. If the expansion functions are associated with the edges of tetrahedron of the mesh instead of their faces, the number of the basis functions introduced by the same mesh is reduced, and therefore, the number of the unknowns in the MoM matrix equation goes down. Such edge-based expansion functions are often referred to as three-dimensional solenoidal expansion functions. They were first proposed by Mendes and Carvalho [33] to reduce the number of basis functions. The edge-based expansion functions have a better convergence rate and higher numerical stability according to Kulkarni et al. [34]. Therefore, the application of the three-dimensional solenoidal functions proposed by [33] in this research area should be considered as a part of the future research effort.

The authors of this work encourage the electromagnetic community to investigate the scattering field solver, to take advantage of its flexibility and to use it as a tool to study scattering problems involving various complicated materials. The results presented in this paper can, by serving as data with which to compare, aid future research in scattering field calculations.

REFERENCES

1. Nurgaliev, T., S. Miteva, A. P. Jenkins, and D. D. Hughes, "Investigation of MW characteristics of HTS microstrip and coplanar resonators with ferrite thin-film components," *IEEE Trans. Microwave Theory Tech.*, Vol. 51, 33–40, Jan. 2003.
2. Tretyakov, S. A. and A. A. Sochava, "Proposed composite material for nonreflecting shields and antenna radomes," *Electron. Lett.*, Vol. 29, No. 12, 1048–1049, Jun. 1993.
3. Lindell, I. V., "Variational method for the analysis of lossless bi-isotropic (nonreciprocal chiral) waveguides," *IEEE Trans. Microwave Theory Tech.*, Vol. 40, 402–405, Feb. 1992.
4. Viitanen, A. J. and I. V. Lindell, "Chiral slab polarization transformer for aperture antennas," *IEEE Trans. Antennas Propagat.*, Vol. 46, 1395–1397, Sep. 1998.
5. Kluskens, M. S. and E. H. Newman, "A microstrip line on a chiral substrate," *IEEE Trans. Microwave Theory Tech.*, Vol. 39, 1889–1891, Nov. 1991.
6. Engheta, N. and D. L. Jaggard, "Electromagnetic chirality and its applications," *IEEE Antennas and Propagation Society Newsletter*, Vol. 30, 6–12, Oct. 1988.
7. Krowne, C. M., "Electromagnetic properties of nonreciprocal composite chiral-ferrite media," *IEEE Trans. Antennas Propagat.*, Vol. 41, 1289–1293, Sep. 1993.
8. Krowne, C. M., "Full-wave spectral Green's function integral-equation calculation of coplanar ferroelectric thin-film transmission structures," *Microwave Opt. Technol. Lett.*, Vol. 26, 187–192, 2000.
9. Krowne, C. M., "Theoretical considerations for finding anisotropic permittivity in layered ferroelectric/ferromagnetic structures from full-wave electromagnetic simulations," *Microwave Opt. Technol. Lett.*, Vol. 28, 63–69, 2001.
10. Krowne, C. M., M. Daniel, S. W. Kirchoefer, and J. M. Pond, "Anisotropic permittivity and attenuation extraction from propagation constant measurements using an anisotropic full-wave Green's function solver for coplanar ferroelectric thin-film devices," *IEEE Trans. Microwave Theory Tech.*, Vol. 50, 537–548, Feb. 2002.
11. Hanson, G. W., "A numerical formulation of dyadic Green's functions for planar bianisotropic media with application to printed transmission lines," *IEEE Trans. Microwave Theory Tech.*, Vol. 44, No. 1, 144–151, Jan. 1996.

12. Cloete, J. H., M. Bingle, and D. B. Davidson, "The role of chirality and resonance in synthetic microwave absorbers," *Int. J. Electron. Comm.*, Vol. 55, No. 4, 223–239, Jul. 2001.
13. Demir, V., A. Elsherbeni, D. Worasawate, and E. Arvas, "A graphical user interface (GUI) for plane wave scattering from a conducting, dielectric or a chiral sphere," Software at ACES web site: http://aces.ee.olemiss.edu, Syracuse, Sep. 2004.
14. Tsalamengas, J., L., "Interaction of electromagnetic waves with general bianisotropic slabs," *IEEE Trans. Microwave Theory Tech.*, Vol. 40, 1870–1878, Oct. 1992.
15. Demir, V., "Electromagnetic scattering from three-dimensional chiral objects using the FDTD method," Ph.D. Dissertation, Syracuse University, 2004.
16. Alu, A., F. Bilotti, and L. Vegni, "Extended method of line procedure for the analysis of microwave components with bianisotropic inhomogeneous media," *IEEE Trans. Antennas Propagat.*, Vol. 51, 1582–1589, Jul. 2003.
17. Yagli, A. F., "Electromagnetic scattering from three-dimensional gyrotropic objects using the transmission line modeling (TLM) method," Ph.D. Dissertation, Syracuse University, 2006.
18. Demir, A., A. Z. Elsherbeni, and E. Arvas, "FDTD formulation for dispersive chiral media using the Z transform method," *IEEE Trans. Antennas Propagat.*, Vol. 53, 3374–3384, Oct. 2005.
19. Bilotti, F., A. Toscano, and L. Vegni, "FEM-BEM formulation for the analysis of cavity-backed patch antennas on chiral substrates," *IEEE Trans. Antennas Propagat.*, Vol. 51, 306–311, Feb. 2003.
20. Valor, L. and J. Zapata, "An efficient finite element formulation to analyze waveguides with lossy inhomogeneous bi-anisotropic materials," *IEEE Trans. Microwave Theory Tech.*, Vol. 44, 291–296, Feb. 1996.
21. Valor, L. and J. Zapata, "A simplified formulation to analyze inhomogeneous waveguide with lossy chiral media using the finite-element method," *IEEE Trans. Microwave Theory Tech.*, Vol. 46, 185–187, Feb. 1998.
22. Mei, C., M. Hasanovic, J. K. Lee, and E. Arvas, "Electromagnetic scattering from an arbitrarily shaped three-dimensional inhomogeneous bianisotropic body," *PIERS Online*, Vol. 3, No. 5, 680–684, 2007.
23. Rao, S. M., D. R. Wilton, and A. W. Glisson, "Electromagnetic scattering by surfaces of arbitrary shape," *IEEE Trans. Antennas Propagat.*, Vol. 30, 409–418, May 1982.

24. Schaubert, D. H., D. R. Wilton, and A. W. Glisson, "A tetrahedral modeling method for electromagnetic scattering by arbitrarily shaped inhomogeneous dielectric bodies," *IEEE Trans. Antennas Propagat.*, Vol. 32, 77–85, Jan. 1984.
25. Wilton, D. R., S. M. Rao, A. W. Glisson, D. H. Schaubert, O. M. Al-Bundak, and C. M. Butler, "Potential integrals for uniform and linear source distributions on polygonal and polyhedral domains," *IEEE Trans. Antennas Propagat.*, Vol. 32, 276–281, Mar. 1984.
26. Carvalho, S. A. and L. S. Mendes, "Scattering of EM waves by inhomogeneous dielectrics with the use of the method of moments and 3-D solenoidal basis functions," *Microwave and Optical Technology Letters*, Vol. 23, No. 1, 42–46, Oct. 1999.
27. Worasawate, D., "Electromagnetic scattering from an arbitrarily shaped three-dimensional chiral body," Ph.D. Dissertation, Syracuse University, 2002.
28. Hasanovic, M., "Electromagnetic scattering from an arbitrarily shaped three-dimensional inhomogeneous chiral body," Ph.D. Dissertation, Syracuse University, 2006.
29. Zhu, X. Q., Y. L. Geng, and X. B. Wu, "Application of MOM-CGM-FFT method to scattering from three-dimensional anisotropic scatterers," *Chinese J. Radio Sci.*, Vol. 17, No. 3, 209–215, 2002 (in Chinese).
30. Geng, Y., X. Wu, and L. Li, "Analysis of electromagnetic scattering by a plasma anisotropic sphere," *Radio Science*, Vol. 38, No. 6, 12-1–12-12, Dec. 2003.
31. Geng, Y. and X. Wu, "A plane electromagnetic wave scattering by a ferrite sphere," *Journal of Electromagnetic Waves and Applications*, Vol. 18, No. 2, 161–179, 2004.
32. Nie, X. C., N. Yuan, L. W. Li, Y. B. Gan, and T. S. Yeo, "A fast combined field volume integral equation solution to EM scattering by 3-D dielectric objects of arbitrary permittivity and permeability," *IEEE Trans. Antennas Propagat.*, Vol. 54, 961–969, Mar. 2006.
33. Mendes, L. S. and S. A. Carvalho, "Scattering of EM waves by homogeneous dielectrics with the use of the method of moments and 3D solenoidal basis functions," *Microwave and Optical Technology Letters*, Vol. 12, No. 6, 327–331, Aug. 1996.
34. Kulkarni, S., R. Lemdiasov, R. Ludwig, and S. Makarov, "Comparison of two sets of low-order basis functions for tetrahedral VIE modeling," *IEEE Trans. Antennas Propagat.*, Vol. 52, 2789–2794, Oct. 2004.